Hindawi
Mathematical Problems in Engineering
Volume 2022, Article ID 3091897, 13 pages
https://doi.org/10.1155/2022/3091897

Research Article

Insights of Heat and Mass Transfer in Magneto-Mixed Convective Sisko Nanofluid over a Wedge with Viscous Dissipation

Yogesh Dadhich,[1] **Reema Jain**,[1] **and Sonam Gyeltshen**[2]

[1]*Department of Mathematics and Statistics, Manipal University Jaipur, Rajasthan 303007, India*
[2]*Department of Humanities and Management, Jigme Namgyel Engineering College, Royal University of Bhutan, Dewathang, Bhutan*

Correspondence should be addressed to Reema Jain; reemajain197@gmail.com and Sonam Gyeltshen; sonamgyeltshen@jnec.edu.bt

Received 7 March 2022; Revised 19 April 2022; Accepted 21 April 2022; Published 23 May 2022

Academic Editor: Arshad Riaz

The current analysis provides the important insights of Sisko nanofluid flow over a wedge with thermal radiation and viscous dissipation effects. The Buongiorno nanofluid model, which includes Brownian movement and thermophoresis, is taken into consideration. Momentum, temperature, and nanoparticle concentration equations are used to simulate the current problem. The suitable similarity variables are applied to the governing partial differential equations (PDEs) which yield the dimensionless ordinary differential equations (ODEs). The MATLAB function bvp4c has been used to resolve the resulting ODEs. The attributes of various flow parameters on the transfer rate of mass, heat, temperature, velocity, and nanoparticle concentration have been explored. The pressure gradient parameter boosts the mass transfer and velocity. Moreover, mixed convection leads to the decrement in thermal and nanoparticle concentration boundary layer. The obtained numerical findings are compared to published results in the literature by considering the particular cases to validate the current study and are seen to be in perfect accord.

1. Introduction

In aerodynamics, geothermal systems, and many other fields, convective flow across a wedge has been discussed extensively. The flow over a wedge is significant because each wedge angle generates a distinct pressure profile, providing insight into boundary layer behaviour in a variety of conditions. Skan [1] was the first to propose a flow arrangement on the wedge. Since then, many researchers have investigated wedge and produced several useful discoveries, including Yih [2], Sattar [3], Turkyilmazoglu [4], Raju and Sandeep [5], Kudenatti et al. [6], Awaludin et al. [7], and many others. Khan and Pop [8] investigated the problem of steady boundary layer flow of nanofluid past a stretchy wedge. For solving the governing system, they employed the implicit finite-difference technique. Rajagopal et al. [9] extended the problem of flow field across a wedge to the problem of non-Newtonian fluid, where fluid of a second grade is examined. Many more studies of the flow field across a wedge were then investigated [10–12]. The steady 2D magnetohydrodynamic wedge flow of micropolar fluid in the presence of fluctuating wall temperature was explored by Ishaq et al. [13]. The boundary layer flows particularly for non-Newtonian fluids over stretched surfaces have been widely discussed by the researchers [14–18]. The Sisko fluid model [19] is one of the most essential models among non-Newtonian fluid models since it accurately describes a few non-Newtonian fluids. It may be assessed as a broad view of Newtonian and power-law fluids. Dadhich and Jain [20] examined some important characteristics of the fluid flow over an exponential surface in the Sisko model. The Falkner–Skan wedge flow of a power-law fluid through a porous material was studied by several researchers, including Kim [21]. Munir et al. [22] investigated convective heat transfer in Sisko nanofluid past a wedge. They applied the unique similarity transformations for converting the physical system. The boundary layer flow of a power-law fluid past a porous stretching wedge was studied by Postelnicu and Pop [23]. Das et al. [24] investigated how different fluid characteristics affect nanofluid flow over a wedge. The flow study was done with the effect of surface slip in account. The wedge flow of a power-law fluid in a porous medium was analyzed by Hassanien et al. [25]. Khan and Shahzad [26] explored Sisko fluid's Falkner–Skan boundary layer movement.

Bano et al. [27] used analytical methods to investigate the stretching wedge of Casson fluid with varied effects.

Enhancement of heat transfer is essential in improving performances and compactness of electronic devices. Usual cooling agents (water, oil, etc.) have relatively small thermal conductivities, and therefore heat transfer is not very efficient. Thus, to augment thermal characteristics, very small size particles (nanoparticles) were added to fluids forming the so-called nanofluids. These suspensions of nanoparticles in fluids have physical and chemical properties depending on the concentration and the shape of particles. It is observed that adding a little amount of nanoparticles to a base fluid increases the thermal conductivity of the fluid significantly. Loganathan et al. [28] investigated 3D flow of viscoelastic nanofluid over an bi-directional stretched surface. They applied the homotopy analysis method and concluded that heat as well as mass transportation is significantly affected by Brownian motion and thermophoresis. Wakif et al. [29] examined the impact of heat and mass transfer mechanisms on convective motion near a heated extending sheet embedded horizontally in a bi-phasic medium containing a certain volume fraction of alumina nanoparticles (Al_2O_3) dispersed completely in a micropolar fluidic medium containing 60% ethylene glycol ($C_2H_6O_2$) ($C_2H_6O_2$ *EG*) and 40% pure water (H_2O). Ashraf et al. [30], using the extended differential quadrature approach, quantitatively investigated the peristaltic flow of a blood-based nanofluid. After completing the thorough literature review, the authors observed that no attempt has been made to fully comprehend the transportation of heat and mass in the Sisko model with suspended nanoparticles over a wedge including viscous dissipation effect. Bhatti and Abdelsalam [31] investigated the peristaltically driven movement of Carreau fluid in a symmetric channel under the effect of a generated and applied magnetic field. They used the tantalum (Ta) and gold (Au) nanoparticles in the hybrid nanofluid with thermal radiation effects. Lubrication theory is used to complete the mathematical framework.

High-temperature plasmas, glass manufacturing, and liquid metal fluids all benefit from heat transfer analysis of boundary layer flow with radiation. These transport phenomena difficulties are particularly non-linear when linked with thermal convection processes. Thermal radiation alters the temperature distribution in the boundary layer at high temperatures, which impacts heat transfer at the wall. Multi-physical radiative-convective fluxes have been the subject of a number of research studies [32–35].

The purpose of this analysis is to examine the magneto-mixed convective Sisko nanofluid over a wedge with viscous dissipation. We extended Sisko nanofluid over a wedge from Macha et al. [36]. But we introduce new similarity variables [22, 26] for constructing a mathematical model. The governing partial differential equations are changed into non-linear ordinary differential equations, which are numerically solved by applying MATLAB bvp4c solver. The obtained numerical findings are compared to published results in the literature by considering the particular cases to validate the current study and are seen to be in perfect accord. The current issue has not yet been published in the scientific literature, and it is important to polymeric manufacturing processes and nuclear waste simulations, to the best of the authors' knowledge.

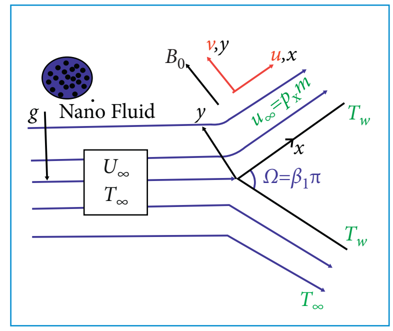

Figure 1: Geometry of physical model.

2. Flow Analysis

In the presence of heat source, radiated laminar flow of Sisko nanofluid is investigated. Heat and mass transport phenomena are considered and discussed. The flow is steady and two-dimensional as illustrated in Figure 1. Rectangular coordinate system is used, where x-axis and y-axis are aligned alongside and perpendicular to wedge surface, respectively. Free stream velocity is considered as u_∞ where $u_\infty(x) = Px^m$ (P is a positive constant). The wedge angle $\Omega = \pi\beta_1$ where $\beta_1 = 2m/m + 1$. Besides, it is assumed that temperature T and nanoparticle fraction C take constant values T_w and C_w, respectively, on the surface of wedge. The ambient temperature and concentration are denoted by T_∞ and C_∞, respectively. A uniform magnetic field B0 is imposed transverse to the wedge surface.

Based on these assumptions, equations for conservation of mass, momentum, thermal energy, and nanoparticle concentration for Sisko nanofluids can be stated as [12, 18, 20]

$$\frac{\partial u}{\partial x} + \frac{\partial v}{\partial y} = 0, \tag{1}$$

$$\begin{aligned} u\frac{\partial u}{\partial x} + v\frac{\partial u}{\partial y} = {} & u_\infty \frac{du_\infty}{dx} + \frac{\epsilon_1}{\rho}\frac{\partial^2 u}{\partial y^2} - \frac{\epsilon_2}{\rho}\frac{\partial}{\partial y}\left(-\frac{\partial u}{\partial y}\right)^n \\ & - \frac{\sigma {B_0}^2 u}{\rho} + g\beta (T - T_\infty)\sin\left(\frac{\Omega}{2}\right) \\ & + g\beta^* (C - C_\infty)\sin\left(\frac{\Omega}{2}\right), \end{aligned} \tag{2}$$

$$\begin{aligned} u\frac{\partial T}{\partial x} + v\frac{\partial T}{\partial y} = {} & \frac{k}{(\rho C_p)_f}\frac{\partial^2 T}{\partial y^2} + \tau\left[D_B\frac{\partial C}{\partial y}\frac{\partial T}{\partial y} + \frac{D_T}{T_\infty}\left(\frac{\partial T}{\partial y}\right)^2\right] \\ & - \frac{1}{(\rho C_p)_f}\frac{\partial q_r}{\partial y} + \frac{Q}{(\rho C_p)_f}(T - T_\infty) \\ & + \frac{\mu}{(\rho C_p)_f}\left(\frac{\partial u}{\partial y}\right)^2 + \frac{\sigma {B_0}^2 u^2}{(\rho C_p)_f}, \end{aligned} \tag{3}$$

$$u\frac{\partial C}{\partial x} + v\frac{\partial C}{\partial y} = D_B\frac{\partial^2 C}{\partial y^2} + \frac{D_T}{T_\infty}\frac{\partial^2 T}{\partial y^2}. \tag{4}$$

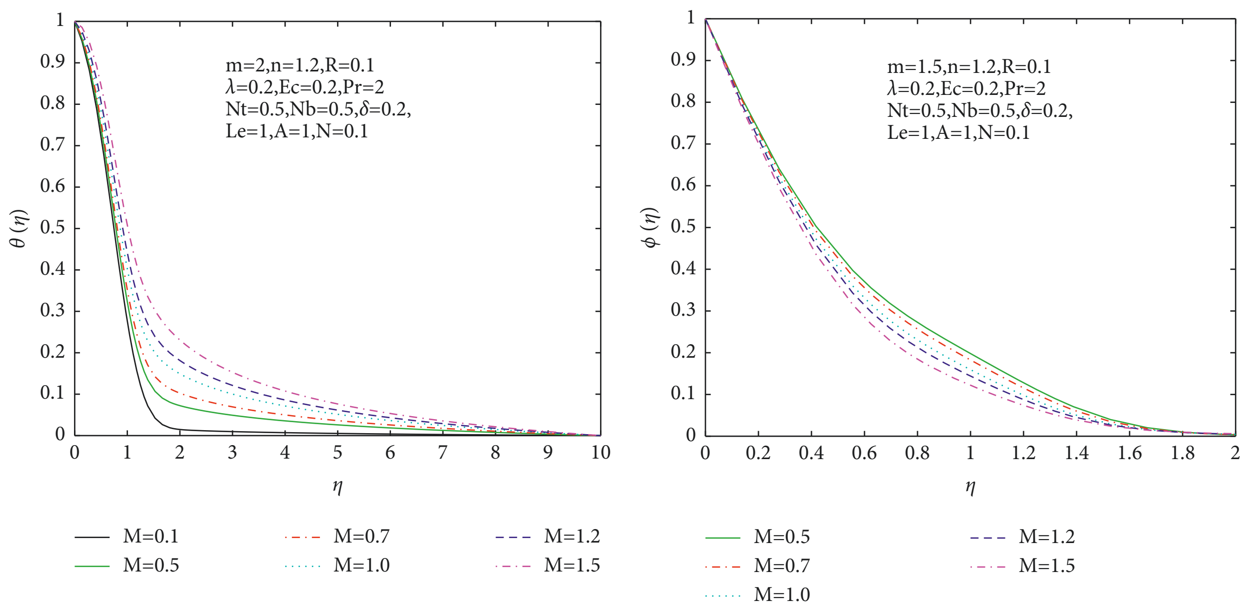

(a) (b)

FIGURE 2: (a) θ Vs M. (b) Φ Vs M.

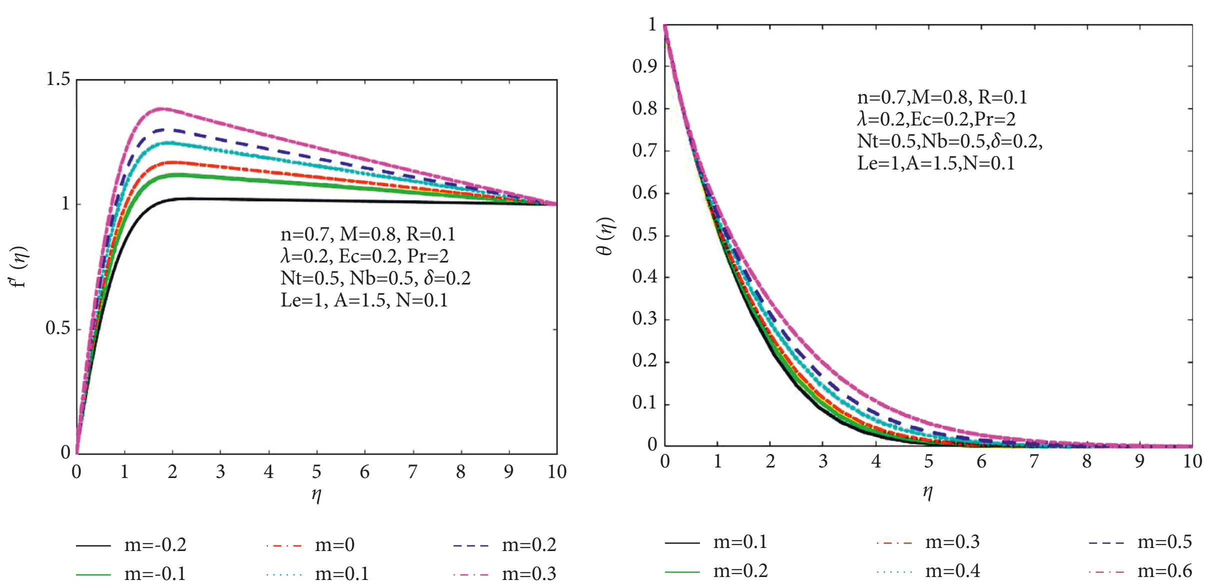

(a) (b)

FIGURE 3: (a) f' Vs m. (b) θ Vs m.

The boundary conditions are

$$\text{at } y = 0\text{: } u = 0; v = 0; T = T_w; C = C_w, \tag{5}$$

$$\text{at } y \longrightarrow \infty\text{: } u = u_\infty = Px^m, v \longrightarrow 0, T \longrightarrow T_\infty, C \longrightarrow C_\infty. \tag{6}$$

Here ϵ_1, ϵ_2, and $n(>0)$ are material constants; $\alpha_f = k/\rho C_p$ is the thermal diffusivity; ϑ is the kinematic viscosity; C_p is the specific heat of the fluid; k is the thermal conductivity; $\tau = (\rho C_p)_p/(\rho C_p)_f$ is the proportion of the heat capacity of nanoparticles to that of the base fluid; D_B is the Brownian diffusion; D_T is the thermophoretic diffusion; and q_r is the radiative heat flux.

The following non-dimensional variables are proposed [22, 26]:

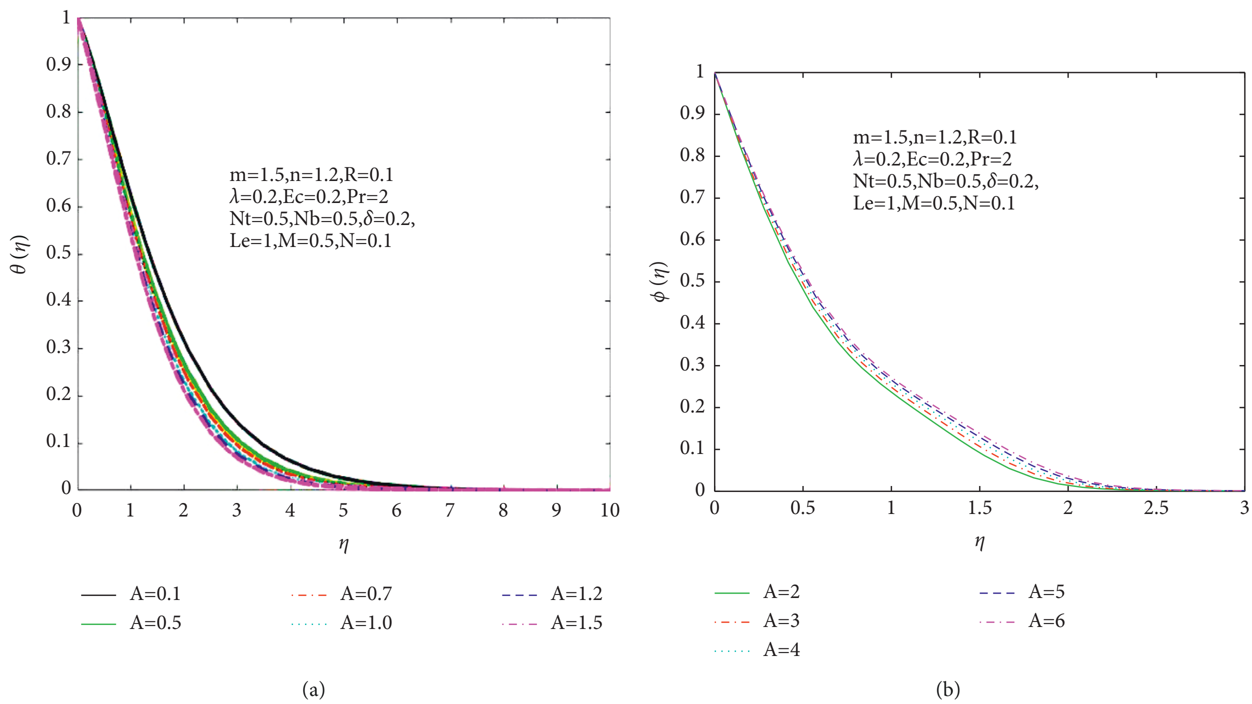

Figure 4: (a) θ Vs A. (b) Φ Vs A.

$$\begin{aligned}
\eta &= \frac{y}{x}(\mathrm{Re}_b)^{1/(n+1)},\\
u &= u_\infty f'(\eta),\\
v &= -u_\infty(\mathrm{Re}_b)^{-1/(n+1)}\left[(m+1)f - \eta f'\right],\\
\theta(\eta) &= \frac{T - T_\infty}{T_w - T_\infty},\\
\phi(\eta) &= \frac{C - C_\infty}{C_w - C_\infty}.
\end{aligned} \tag{7}$$

The Rosseland diffusion flux model can be defined as follows:

$$q_r = -\frac{4\sigma^*}{3k^*}\frac{\partial T^4}{\partial y}. \tag{8}$$

Usually, T^4 is expressed as a linear function of temperature, and applying Taylor's expansion (ignoring higher-order terms), it takes the form

$$T^4 = 4T_\infty^3 - 3T_\infty^4. \tag{9}$$

The following set of ODEs may be obtained by using (7), (8), and (9) in equations (2)–(6):

$$\begin{aligned}
&Af''' + n(-f'')^{n-1}f''' + Mf' - mf'^2 + (m+1)ff''\\
&\quad + m + \lambda\{\theta + N\phi\}\sin\left(\frac{\Omega}{2}\right) = 0,\\
&\left(1 + \frac{4R}{3}\right)\theta'' + P_r\left[(m+1)f\theta' + N_b\theta'\phi' + N_t\theta'^2\right] + \delta P_r\theta\\
&\quad + MP_rE_cf'^2 + E_cf''^2 = 0,\\
&\phi'' + P_rL_e(m+1)f\phi' + \left(\frac{N_t}{N_b}\right)\theta'' = 0.
\end{aligned} \tag{10}$$

Transformed boundary conditions are

$$\begin{aligned}
&\text{at } \eta = 0\text{: } f(\eta) = 0, f'(\eta) = 0, \theta(\eta) = 1, \phi(\eta) = 1,\\
&\text{at } \eta \longrightarrow \infty\text{: } f'(\eta) = 1, f(\eta) = 1, \theta(\eta) = 0, \phi(\eta) = 0.
\end{aligned} \tag{11}$$

Here prime implies the differentiation with respect to η, and the non-dimensional terms are described as

$$\begin{aligned}
&M = \frac{\sigma B_0^2 x}{\rho u_\infty}; P_r = \frac{\vartheta}{\alpha_f}; N_b = \frac{\tau D_B(C_w - C_\infty)}{\vartheta};\\
&N_t = \frac{\tau D_T(T_w - T_\infty)}{\vartheta T_\infty}; L_e = \frac{\alpha_f}{D_B}; R = \frac{4\sigma^* T_\infty{}^3}{k^* k},\\
&\delta = \frac{Qx}{\rho c_p u_\infty}; E_c = \frac{(u_\infty)^2}{(c_p)_f(T_w - T_\infty)}; \mathrm{Re}_a = \frac{\rho x u_\infty}{\epsilon_1};\\
&R_{e_b} = \frac{\rho x (u_\infty)^{(2-n)}}{\epsilon_2}; A = \frac{(\mathrm{Re}_b)^{2/(n+1)}}{\mathrm{Re}_a},\\
&N = \frac{\beta^*(C_w - C_\infty)}{\beta(T_w - T_\infty)}; \lambda = \frac{G_{r_x}}{(\mathrm{Re}_x)^2}; G_{r_x} = \frac{g\beta(T_w - T_\infty)x^3}{4\vartheta^2}.
\end{aligned} \tag{12}$$

2.1. Coefficients of Heat and Mass Transport. The main goal of this study is to figure out what factors are important to engineers when they deal with heat and nanoparticle mass transfer. The engineering interests of the physical quantities are defined below: local Nusselt number $N_{u_x} = (xq_w/k(T_w - T_\infty))_{y=0}$ and local nanofluid Sherwood number is given by $Sh_x = (xq_w/D_B(C_w - C_\infty))_{y=0}$; where $q_w = -k(\partial T/\partial y)_{y=0}$ is wall heat flux. Using above-mentioned transformations, these

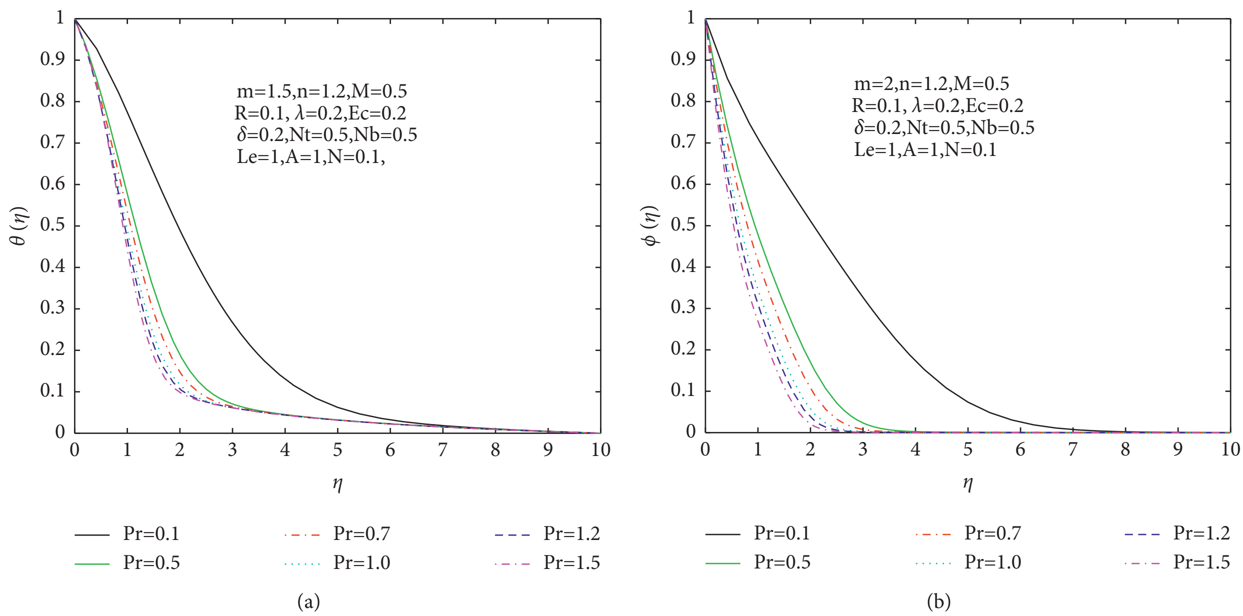

Figure 5: (a) θ Vs Pr. (b) Φ Vs Pr.

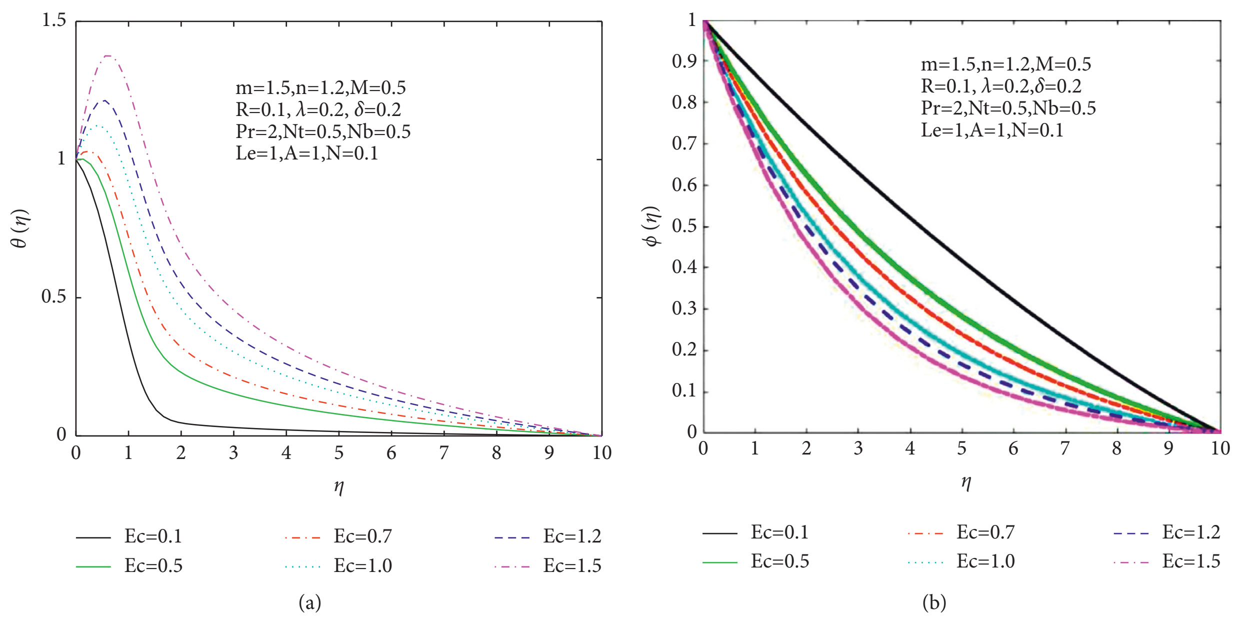

Figure 6: (a) θ Vs Ec. (b) Φ Vs Ec.

parameters will reduce to $(\mathrm{Re_b})^{-1/(n+1)} N_{u_x} = -(1 + 4R/3)\theta'(0)$ and $(\mathrm{Re_b})^{-1/(n+1)} Sh_x = -\phi'(0)$.

3. Numerical Computation

The above-mentioned system of non-linear ODEs along with boundary conditions is solved by applying MATLAB bvp4c code. Thus, the system is converted to first-order ODEs using the mathematical algorithm which is appended below ((13)–(29)). "Boundary conditions defined at infinity are addressed by fixing it at a finite value, for example, $\eta_\infty = 10$ implies that variable is confined in $0 \le \eta \le 10$". Calculations are performed numerically using an interval $\Delta\eta = 0.01$, 10^{-3} is a convergent criterion to repeated and attain the numeric solution.

$$f = g_1, \tag{13}$$

$$f' = g_2, \tag{14}$$

$$f'' = g_3, \tag{15}$$

$$f''' = g_3', \tag{16}$$

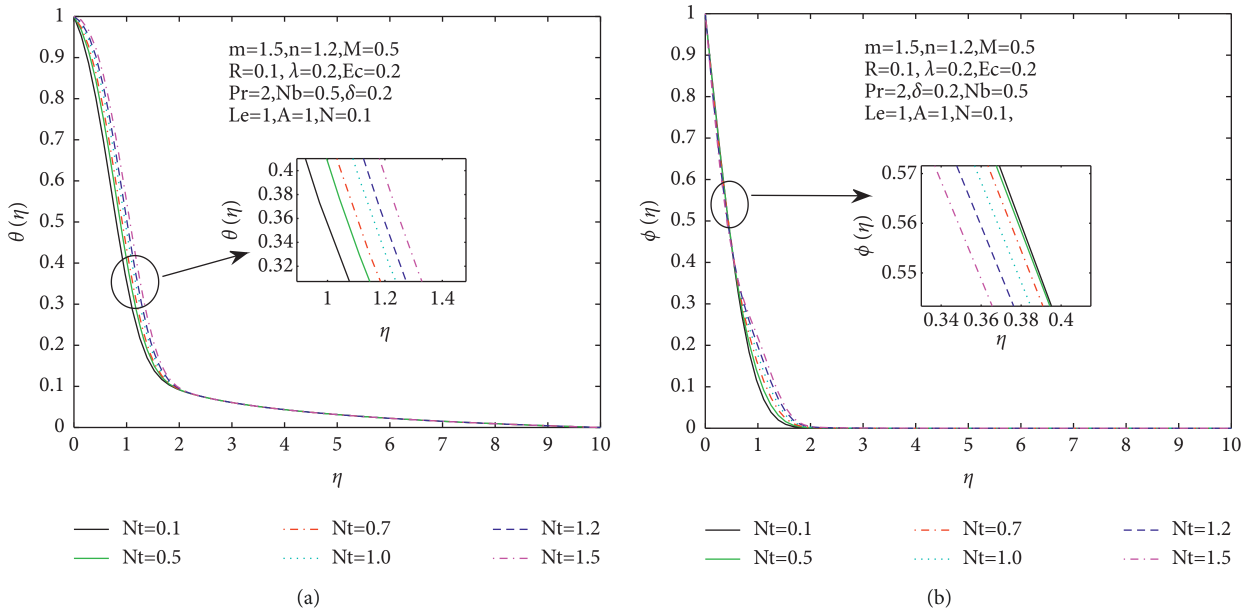

Figure 7: (a) θ Vs N_t. (b) Φ Vs N_t.

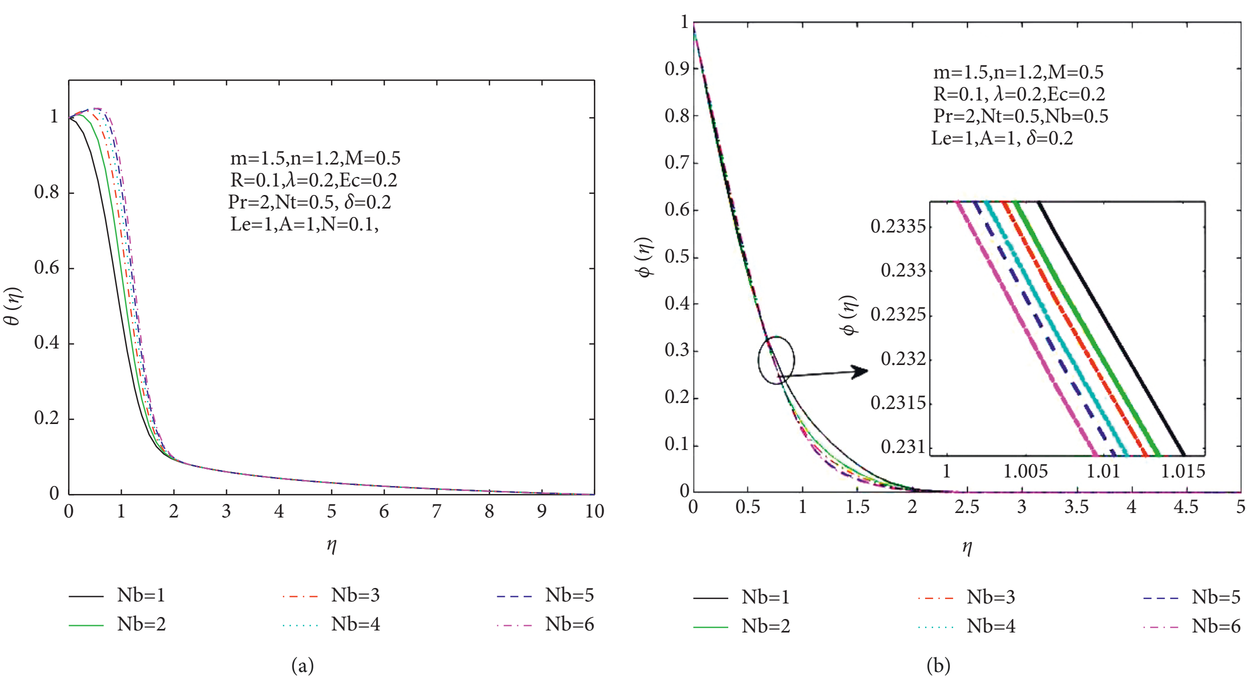

Figure 8: (a) θ Vs N_b. (b) Φ Vs N_b.

$$\theta = g_4, \tag{17}$$

$$\theta' = g_5, \tag{18}$$

$$\theta'' = g_5', \tag{19}$$

$$\phi = g_6, \tag{20}$$

$$\phi' = g_7, \tag{21}$$

$$\phi'' = g_7', \tag{22}$$

$$f''' = \frac{{g_2}^2 m - M g_2 - m - (m+1) g_1 g_3 - \lambda \{g_4 + N g_6\} \sin(\Omega/2)}{A + (-1)^{n-1} n (g_3)^{n-1}}, \tag{23}$$

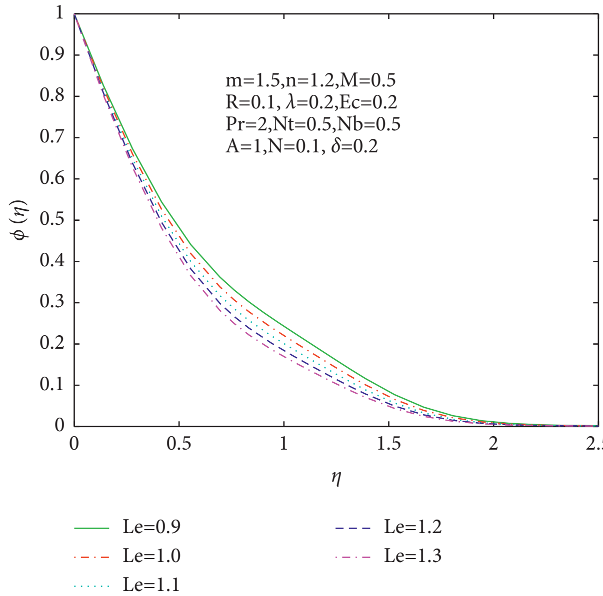

Figure 9: Φ Vs *Le*.

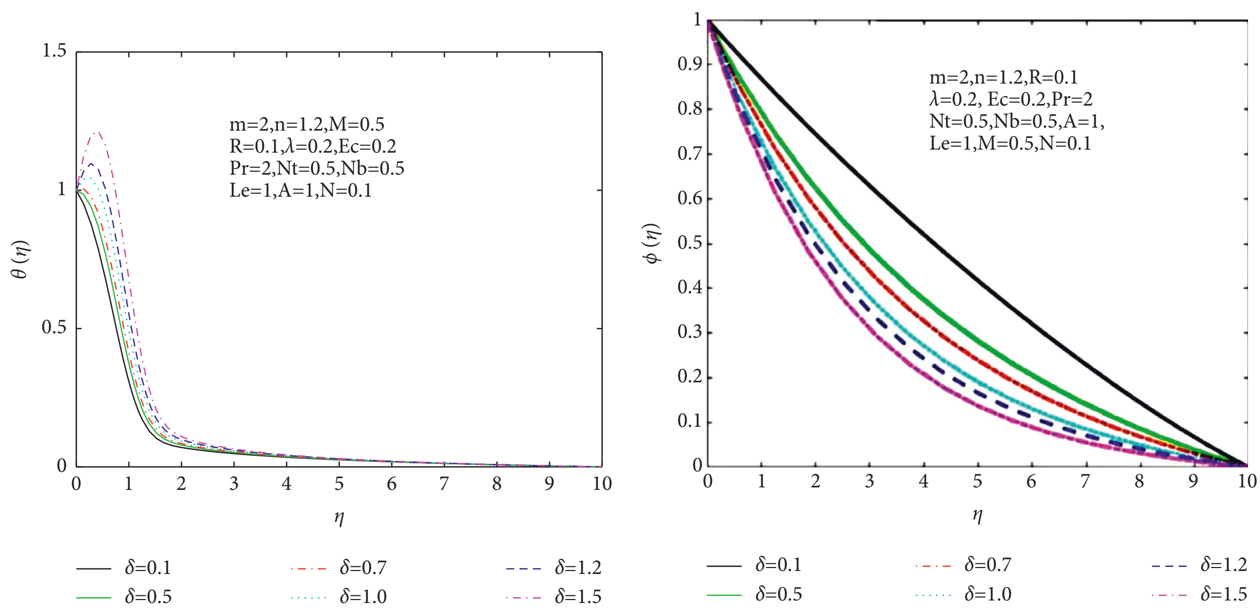

(a) (b)

Figure 10: (a) θ Vs δ. (b) Φ Vs δ.

$$\theta'' = g_5{}' = \frac{\left[P_r (m+1) g_1 g_5 + \delta P_r g_4 + E_c (g_3)^2 + M P_r E_c g_2^2 + P_r \left(N_b g_5 g_7 + N_t g_5^2\right)\right]}{-(1+4\mathrm{R}/3)}, \tag{24}$$

$$\phi'' = g_7' = -\left[P_r L_e (m+1) g_1 g_7 + \frac{N_t}{N_b} g_5'\right]. \tag{25}$$

Using boundary conditions:

$$g_0(1) = 0, g_0(2) = 0, g_0(4) - 1 = 0, g_0(6) - 1 = 0, \tag{26}$$

$$g_1(2) - 1 = 0, g_1(1) - 1 = 0, g_1(4) = 0, g_1(6) = 0. \tag{27}$$

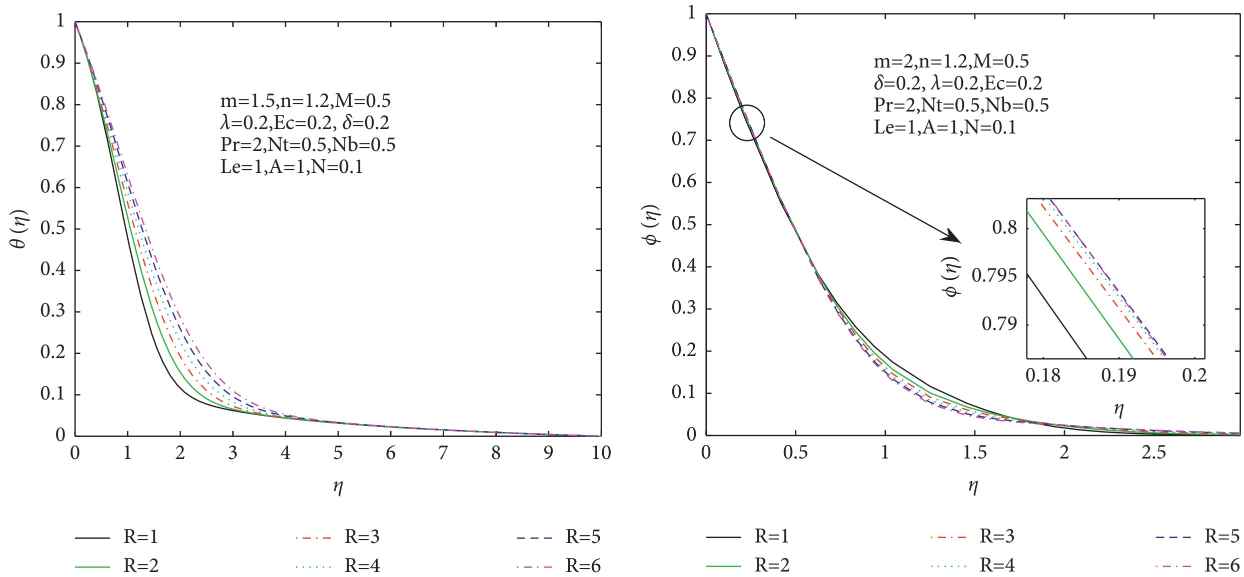

(a) (b)

Figure 11: (a) θ vs R. (b) Φ Vs R.

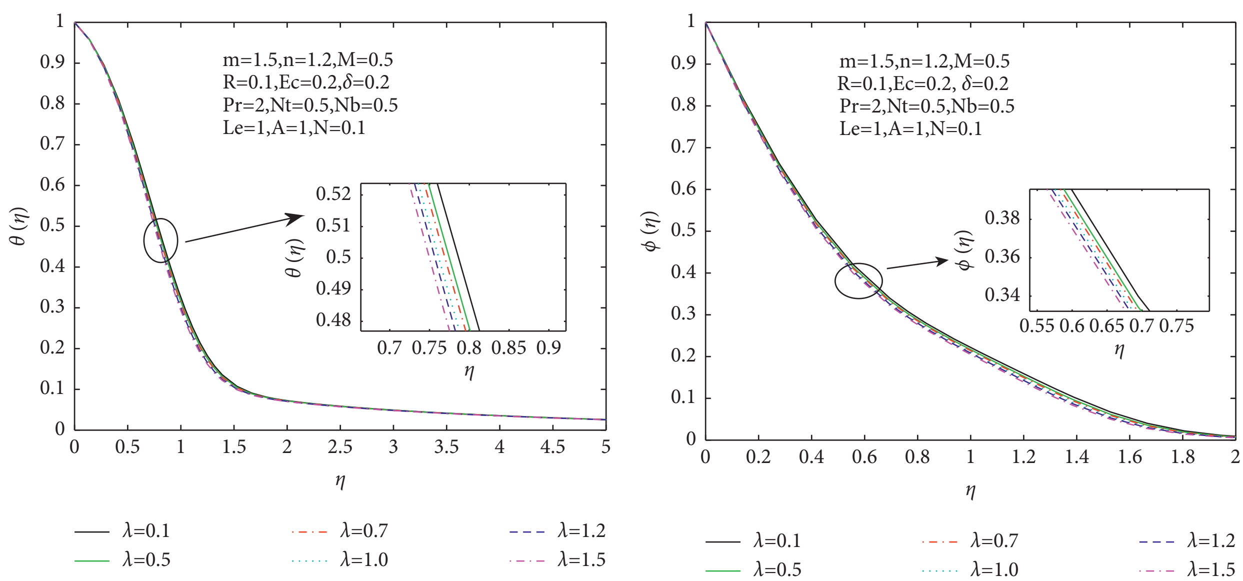

(a) (b)

Figure 12: (a) θ Vs λ. (b) Φ Vs λ.

4. Result and Discussion

In this section, the impact of numerous physical parameters on temperature and concentration is demonstrated. The fixed values of physical parameters are $m = 1, M = 0.8, n = 1, R = 0.1, Ec = 0.2, A = 1, N = 0.1, Nb = 0.5, Nt = 0.5, Le = 1, \lambda = 0.2, \delta = 0.2$. These findings are summarized in Figures 2–17 and Tables 1 and 2. Figures 2(a) and 2(b) illustrate the graphs of temperature (θ) and concentration (ϕ) for different M. As strength of magnetic field is increased, it increases resistive force. Therefore, additional heat is produced which causes high temperature and concentration of nanoparticles decreases. The impact of m on fluid flow and heat is represented by Figures 3(a) and 3(b). This variation is due to m, which is associated with pressure gradient. Increasing values of m indicate a promising pressure gradient which improves the flow. Fluid temperature is also influenced by wedge angle. Figures 4(a) and 4(b) demonstrate the effect of A (material parameter) on θ and ϕ. Due to the fact that the material parameter has an inverse relationship with consistency index b (fluid's viscosity). As A increases, fluid viscosity decreases which causes less resistance for the fluid

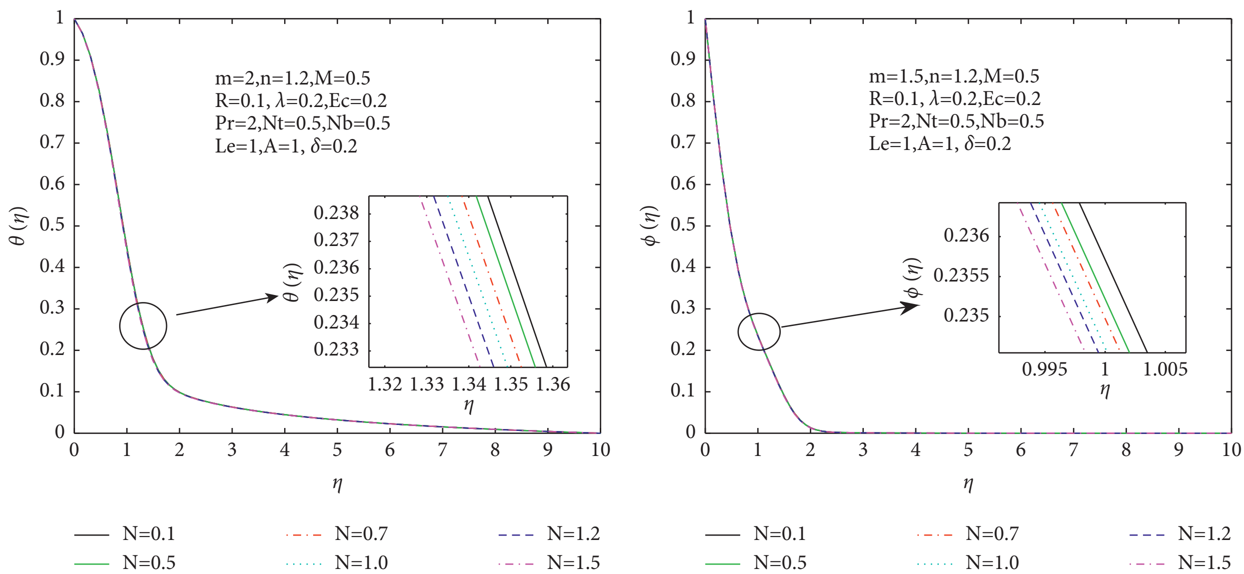

(a)

(b)

Figure 13: (a) θ Vs N. (b) Φ Vs N.

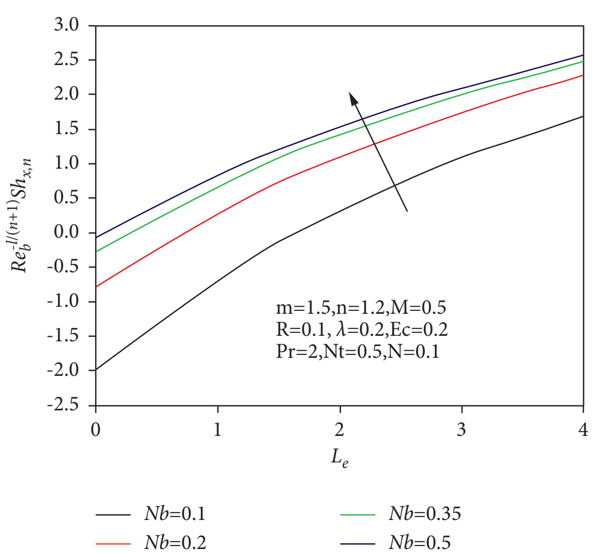

Figure 14: Change in $-\phi'(0)$ with L_e and N_b.

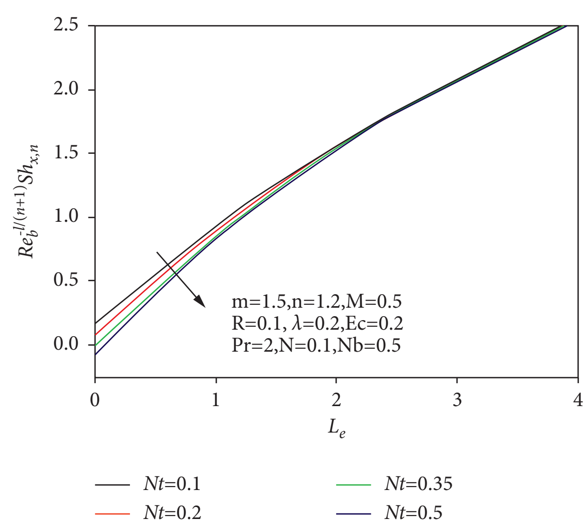

Figure 15: Change in $-\phi'(0)$ withL_e and N_t.

to move, and this increases the fluid velocity. As a result, an increase in material parameter A results in a decay of the temperature profile and a rise in concentration.

Figures 5(a) and 5(b) illustrate the influence of Pr on the distribution of heat and nanoparticle concentrations, respectively. The graph demonstrates that when Pr grows, the temperature of the fluid drops. Since Pr is inversely proportional to thermal diffusivity. Consequently, the temperature drops and the nanoparticle concentration is also reduced as Pr rises. The change in temperature and concentration as Ec varies is exhibited in Figures 6(a) and 6(b). It explains that increase in Ec enhances the temperature of fluid. As energy is accumulated in fluid due to frictional heating, nanoparticle concentration decreases. Figures 7(a) and 7(b) depict the effect of N_t on θ and ϕ. Growing N_t causes particles to move more quickly, raising the fluid temperature. Furthermore, when N_t increases, the nanoparticle concentration nearest to the surface drops and rises away from it. As N_t increases, more particles are expelled off the heated surface, causing the concentration to increase. Additionally, as seen in Figures 8(a) and 8(b), the parameter N_b has an effect on the temperature and concentration of nanoparticles. With increasing N_b values, the concentration of nanoparticles in fluid falls.

Figure 9 shows a shift in concentration as Le increases. Evidently, ϕ reduces as Le increases. This is because Le has an inverse relationship with D_B, which is associated with N_b. Thus, an increase in Le lowers the thermal diffusivity, causing a decrease in the speed in boundary layer area. Figures 10(a) and 10(b) illustrate temperature and concentration patterns for different δ (which is >0). By

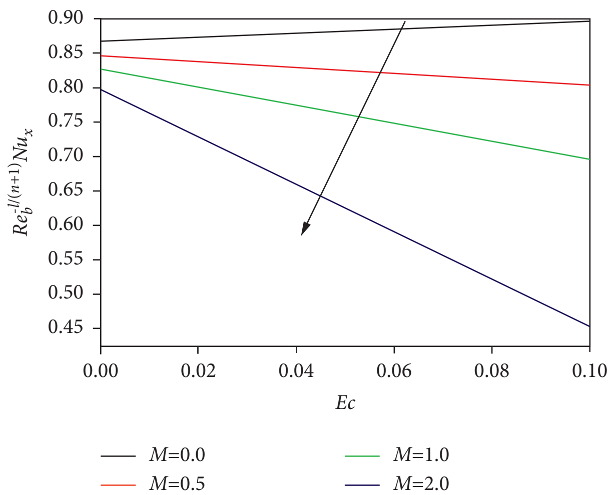

FIGURE 16: Change in $-\theta'(0)$ with M and Ec.

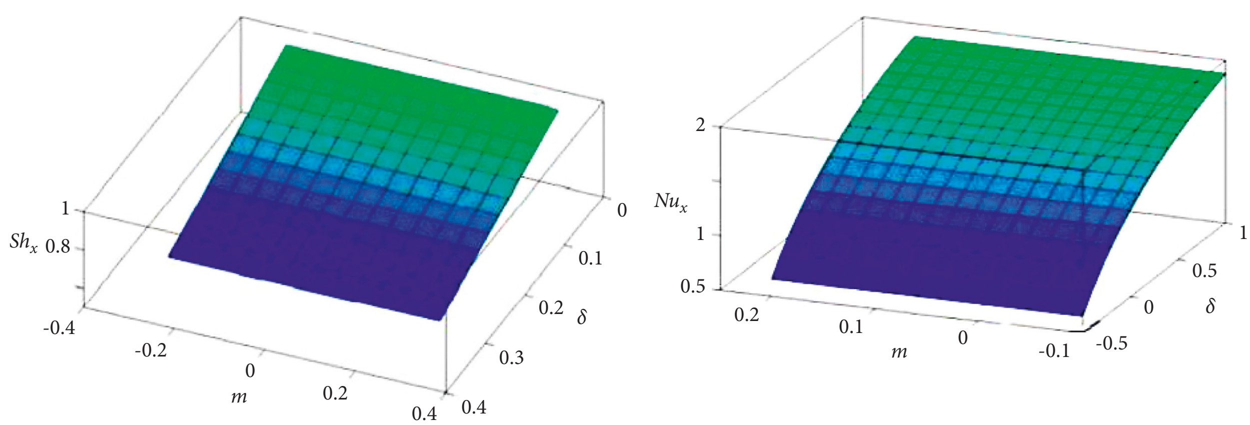

FIGURE 17: (a) 3D plot of $(\mathrm{Re}_b)^{-1/(n+1)}Sh_x$ for m and δ. (b) 3D plot of $(\mathrm{Re}_b)^{-1/(n+1)}N_{u_x}$ for m and δ.

TABLE 1: Comparative study of $f''(0)$ and $-\theta'(0)$ of $M=0.5$, $Ec=0.2$, $R=0.1$, and $A=1$.

m	Gaffar et al. [37]		Current study	
	$\mathbf{f}''(0)$	$-\theta'(0)$	$\mathbf{f}''(0)$	$-\theta'(0)$
0.1	0.4914	0.2083	0.4900	0.2292
0.2	0.5589	0.2122	0.5569	0.2362
0.3	0.6259	0.2162	0.6213	0.2376
0.4	0.6917	0.2202	0.6901	0.2426

enhancing δ, the temperature scales are increased but reduction is observed in concentration values. Consequently, the concentration decreases. A similar trend is observed for temperature and concentration when R increases as shown in Figures 11(a) and 11(b). High values of R result in a higher temperature of fluid.

Figures 12(a) and 12(b) indicate temperature and concentration profiles with different λ. Clearly, it is concluded that increment in λ causes the decline in fluid's temperature and similar behaviour is observed for the concentration. Likewise, the increasing values of N reduce both temperature and concentration as depicted in Figures 13(a) and 13(b). Figure 14 shows that increment in L_e causes decay in concentration profile. Hence, nanofluid's Sherwood number $-\phi'(0)$ is enhanced. Instead, Figure 15 reveals that the nanofluid's Sherwood number decreases with N_t. Also, Figure 16 shows the diminishing tendency of local Nusselt number as Ec and M increase. Figures 17(a) and 17(b) show that heat and mass transfer rates increase as m increases. Increasing δ values cause a decrease in heat transfer while mass transfer increases.

Table 1 compares the local skin friction and Nusselt number for different m, and it is pretty evident that the conclusions of the current analysis are consistent with those of other researchers. Table 2 shows the variation of heat and mass transfer rate with respect to change in m, N, Pr, λ, and δ. It is perceived that heat transfer rate shows an increasing behaviour when the values of all the parameters are rising; however, when δ is increasing, the heat transfer rate is decreasing. Also, the rate of mass transfer enhances with the increase of the value of m.

Table 2: Nu_x and Sh_x for various values of m, N, Pr, λ, and δ taking $n = 1.2$, $M = 0.5$, $Ec = 0.2$, $R = 0.1$, and $A = 1$.

m	N	Pr	λ	δ	$(\mathrm{Re}_b)^{-1/(\mathbf{n}+1)}\mathbf{N}_{\mathbf{u}_x}$ (heat transfer rate)	$(\mathrm{Re}_b)^{-1/(\mathbf{n}+1)}\mathbf{Sh}_{\mathbf{x}}$ (mass transfer rate)
0.2	0.1	0.7	0.2	0.2	0.2362	0.3235
	0.5				0.2372	0.3265
	1.0				0.2383	0.3295
	0.5	0.5	0.2		0.2321	0.3251
		1.0			0.2431	0.3249
		2.0			0.2659	0.3245
	0.1	0.7	0.1		0.2336	0.3261
			0.2		0.2362	0.3335
			0.5		0.2384	0.3392
0.2	0.1	0.7	0.2		0.2362	0.3235
0.3					0.2373	0.3398
0.4					0.2426	0.3531
0.2	0.1	0.7	0.2	0.0	0.2726	0.3235
				0.2	0.2362	0.3236
				0.4	0.2203	0.3342

5. Conclusion

In the present work, analysis of heat and mass transfer in the Sisko model with suspended nanoparticles over a wedge including viscous dissipation effect is investigated. The effects of the wedge angle parameter, nanoparticle volume fraction, radiation, heat generation/absorption, and other variables are explored and presented graphically. For many physical parameters, numerical values of rate of heat and mass transport are provided, and noteworthy aspects are explained in depth. The obtained numerical findings are compared to published results in the literature by considering the particular cases to validate the current study and are seen to be in perfect accord. The following is a summary of the key findings of this study:

(i) The higher values of pressure gradient parameter (m) lead to the rising phenomena in the velocity profile.

(ii) While a material parameter (A) is increased, the temperature profile decays and the concentration rises.

(iii) Prandtl and Schmidt numbers affect mass concentration reversely.

(iv) Thermal and solutal boundary layers are declined due to the augmentation in mixed convection parameter (λ).

(v) Increasing values of magnetic field and Eckert number will produce a diminishing behaviour in heat transfer rate.

(vi) Mass transfer rate is more pronounced for higher values of pressure gradient parameter.

Abbreviations

A: Material parameter (dimensionless)
B_0: Magnetic field strength (kg s^{-2}A^{-1})
C: Concentration (kg m^{-3})
C_∞: Ambient concentration (kg m^{-3})
C_w: Sheet concentration (kg m^{-3})
c_p: Specific heat (J kg^{-1} K^{-1})
D_B: Coefficient of Brownian diffusion (m^2 s^{-1})
D_T: Coefficient of thermophoretic diffusion (m^2 s^{-1})
E_c: Eckert number (dimensionless)
k: Thermal conductivity (W m^{-1} K^{-1})
L_e: Lewis parameter (dimensionless)
m: Pressure gradient parameter
M: Magnetic field parameter (dimensionless)
N: Concentration to thermal buoyancy ratio parameter
N_b: Brownian diffusion parameter (dimensionless)
N_t: Thermophoresis parameter (dimensionless)
Nu_x: Local Nusselt number (dimensionless)
P_r: Prandtl number (dimensionless)
q_r: Radiative heat flux (Wm^{-2})
R: Radiation parameter (dimensionless)
Re_a, Re_b: Local Reynolds numbers (dimensionless)
Sh_x: Sherwood number (dimensionless)
T: Fluid temperature (K)
T_w: Sheet temperature (K)
T_∞: Ambient fluid temperature (K)
u, v: Velocity components (m s^{-1})
x, y: Cartesian coordinates (m)
G_{r_x}: Local Grashof number (dimensionless)
α_f: Thermal diffusivity $(m^2 s^{-1})$
β: Coefficient of thermal expansion (K^{-1})
β^*: Coefficient of concentration expansion
β_1: Wedge angle parameter
δ: Heat source/sink parameter (dimensionless)
η: Similarity parameter (dimensionless)
θ: Temperature similarity function (dimensionless)
ϕ: Concentration similarity function (dimensionless)
λ: Mixed convection parameter (dimensionless)
ϑ: Kinematic viscosity $(m^2 s^{-1})$
ρ: Density (kg m^{-1})
τ: Ratio of the effective heat capacity
σ: Electrical conductivity (S m)
f: Fluid phase
∞: Ambient condition
w: Surface condition.

Data Availability

No data were used to support this study.

Conflicts of Interest

The authors declare that there are no conflicts of interest.

Authors' Contributions

All authors contributed equally to this work. All authors have read and approved the final version of the manuscript.

References

[1] F. Skan, "Philosophical," *Magazine*, vol. 12, pp. 865–896, 1931.

[2] K. A. Yih, "Uniform suction/blowing effect on forced convection about a wedge: uniform heat flux," *Acta Mechanica*, vol. 128, no. 3-4, pp. 173–181, 1998.

[3] M. A. Sattar, "A local similarity transformation for the unsteady twodimensional hydrodynamic boundary layer equations of a flow past a wedge," *International Journal of Applied Mathematics and Mechanics*, vol. 7, pp. 15–28, 2011.

[4] M. Turkyilmazoglu, "Slip flow and heat transfer over a specific wedge: an exactly solvable Falkner-Skan equation," *Journal of Engineering Mathematics*, vol. 92, no. 1, pp. 73–81, 2015.

[5] C. S. K. Raju and N. Sandeep, "Nonlinear radiative magnetohydrodynamic Falkner-Skan flow of Casson fluid over a wedge," *Alexandria Engineering Journal*, vol. 55, no. 3, pp. 2045–2054, 2016.

[6] R. B. Kudenatti, S. R. Kirsur, A. L. Nargund, and N. M. Bujurke, "Similarity solutions of the MHD boundary layer flow past a constant wedge within porous media," *Mathematical Problems in Engineering*, vol. 2017, Article ID 1428137, 11 pages, 2017.

[7] I. S. Awaludin, A. Ishak, and I. Pop, "On the stability of MHD boundary layer flow over a stretching/shrinking wedge," *Scientific Reports*, vol. 8, no. 1, pp. 13622–13628, 2018.

[8] W. A. Khan and I. Pop, "Boundary layer flow past a wedge moving in a nanofluid," *Mathematical Problems in Engineering*, vol. 20137 pages, Article ID 637285, 2013.

[9] K. R. Rajagopal, A. S. Gupta, and T. Y. Na, "A note on the falkner-skan flows of a non-Newtonian fluid," *International Journal of Non-linear Mechanics*, vol. 18, no. 4, pp. 313–320, 1983.

[10] M. J. Martin and I. D. Boyd, "Falkner-Skan flow over a wedge with slip boundary conditions," *Journal of Thermophysics and Heat Transfer*, vol. 24, no. 2, pp. 263–270, 2010.

[11] K.-L. Hsiao, "MHD mixed convection for viscoelastic fluid past a porous wedge," *International Journal of Non-linear Mechanics*, vol. 46, no. 1, pp. 1–8, 2011.

[12] M. M. Rahman, M. A. Al-Lawatia, I. A. Eltayeb, and N. Al-Salti, "Hydromagnetic slip flow of water based nanofluids past a wedge with convective surface in the presence of heat generation (or) absorption," *International Journal of Thermal Sciences*, vol. 57, pp. 172–182, 2012.

[13] A. Ishak, R. Nazar, and I. Pop, "MHD Boundary-layer flow of a micropolar fluid past a wedge with variable wall temperature," *Acta Mechanica*, vol. 196, no. 1-2, pp. 75–86, 2008.

[14] T. Hayat, R. Sajjad, T. Muhammad, A. Alsaedi, and R. Ellahi, "On MHD nonlinear stretching flow of Powell-Eyring nanomaterial," *Results in Physics*, vol. 7, pp. 535–543, 2017.

[15] K. Loganathan, S. Sivasankaran, M. Bhuvaneswari, and S. Rajan, "Second-order slip, cross-diffusion and chemical reaction effects on magneto-convection of Oldroyd-B liquid using Cattaneo-Christov heat flux with convective heating," *Journal of Thermal Analysis and Calorimetry*, vol. 136, no. 1, pp. 401–409, 2019.

[16] R. S. Saif, T. Hayat, R. Ellahi, T. Muhammad, and A. Alsaedi, "Stagnation-point flow of second grade nanofluid towards a nonlinear stretching surface with variable thickness," *Results in Physics*, vol. 7, pp. 2821–2830, 2017.

[17] T. Hayat, R. S. Saif, R. Ellahi, T. Muhammad, and B. Ahmad, "Numerical study for Darcy-Forchheimer flow due to a curved stretching surface with Cattaneo-Christov heat flux and homogeneous-heterogeneous reactions," *Results in Physics*, vol. 7, pp. 2886–2892, 2017.

[18] Y. Dadhich, R. Jain, A. R. Kaladgi, M. Alwetaishi, A. Afzal, and C. A. Saleel, "Thermally radiated Jeffery fluid flow with nanoparticles over a surface of varying thickness in the influence of heat source," *Case Studies in Thermal Engineering*, vol. 28, no. 1, Article ID 101549, 2021.

[19] A. W. Sisko, "The flow of lubricating greases," *Industrial and Engineering Chemistry*, vol. 50, no. 12, pp. 1789–1792, 1958.

[20] Y. Dadhich and R. Jain, "Numerical solution of magnetohydrodynamic flow and heat transfer of sisko fluid over an exponential stretching sheet," *Journal of Physics: Conference Series*, vol. 1504, no. 1, Article ID 012005, 2020.

[21] Y. J. Kim, "The Falkner-Skan wedge flows of power-law fluids embedded in a porous medium," *Transp Porous Media*, vol. 44, no. 2, pp. 267–279, 2001.

[22] A. Munir, A. Shahzad, and M. Khan, "Convective flow of Sisko fluid over a wedge with viscous dissipation," *Journal of the Brazilian Society of Mechanical Sciences and Engineering*, vol. 38, no. 2, pp. 581–587, 2016.

[23] A. Postelnicu and I. Pop, "Falkner-Skan boundary layer flow of a power-law fluid past a stretching wedge," *Applied Mathematics and Computation*, vol. 217, no. 9, pp. 4359–4368, 2011.

[24] K. Das, N. Acharya, and P. K. Kundu, "Influence of variable fluid properties on nanofluid flow over a wedge with surface slip," *Arabian Journal for Science and Engineering*, vol. 43, no. 5, pp. 2119–2131, 2018.

[25] I. A. Hassanien, A. A. Abdullah, and R. S. R. Gorla, "Flow and heat transfer in a power-law fluid over a nonisothermal stretching sheet," *Mathematical and Computer Modelling*, vol. 28, no. 9, pp. 105–116, 1998.

[26] M. Khan and A. Shahzad, "Falkner-Skan boundary layer flow of a Sisko Fluid," *Zeitschrift für Naturforschung A*, vol. 67, no. 8-9, pp. 469–478, 2012.

[27] N. Bano, B. B. Singh, and S. R. Sayyed, "MHD heat transfer flow of Casson fluid with velocity and thermal slips over a stretching wedge in the presence of thermal radiation," *Diffusion Foundations*, vol. 26, pp. 1–22, 2020.

[28] K. Loganathan, N. Alessa, and S. Kayikci, "Heat transfer analysis of 3-D viscoelastic nanofluid flow over a convectively heated porous Riga plate with Cattaneo-Christov double flux," *Frontiers in Physics*, vol. 9, 2021.

[29] A. Wakif, M. Zaydan, A. Ali Saleh, T. Muhammad, and R. Sehaqui, "New insights into the dynamics of alumina-(60% ethylene glycol + 40% water) over an isothermal stretching sheet using a renovated Buongiorno's approach: a numerical GDQLLM analysis," *International Communications in Heat and Mass Transfer*, vol. 133, Article ID 105937, 2022.

[30] M. U. Ashraf, M. Qasim, A. Wakif, M. I. Afridi, and I. L. Animasaun, "A generalized differential quadrature algorithm for simulating magnetohydrodynamic peristaltic flow of blood-based nanofluid containing magnetite nanoparticles: a physiological application," *Numerical Methods for Partial Differential Equations*, vol. 38, pp. 666–692, 2022.

[31] M. M. Bhatti and S. I. Abdelsalam, "Bio-inspired Peristaltic Propulsion of Hybrid Nanofluid Flow with Tantalum (Ta) and Gold (Au) Nanoparticles under Magnetic Effects," *Waves in Random and Complex Media*, 2021.

[32] N. Acharya, "Spectral quasi linearization simulation on the radiative nanofluid spraying over a permeable inclined

spinning disk considering the existence of heat source/sink," *Applied Mathematics and Computation*, vol. 411, Article ID 126547, 2021.

[33] K. Loganathan and S. Rajan, "An entropy approach of Williamson nanofluid flow with Joule heating and zero nanoparticle mass flux," *Journal of Thermal Analysis and Calorimetry*, vol. 141, no. 6, pp. 2599–2612, 2020.

[34] Z. Sabir, A. Imran, M. Umar et al., "A numerical approach for 2-D sutterby fluid-flow bounded at a stagnation point with an inclined magnetic field and thermal radiation impacts," *Thermal Science*, vol. 25, pp. 1975–1987, 2021.

[35] K. Loganathan, K. Mohana, M. Mohanraj, P. Sakthivel, and S. Rajan, "Impact of third-grade nanofluid flow across a convective surface in the presence of inclined Lorentz force: an approach to entropy optimization," *Journal of Thermal Analysis and Calorimetry*, vol. 144, no. 5, pp. 1935–1947, 2020.

[36] M. Madhu, C. S. Reddy, and N. Kishan, "Magnetohydrodynamic flow and heat transfer to Sisko nanofluid over a wedge," *International Journal of Fluid Mechanics Research*, vol. 44, no. 1, pp. 1–13, 2017.

[37] S. A. Gaffar, V. R. Prasad, and E. Keshava Reddy, "Mixed convection boundary layer flows of a non-Newtonian Jeffrey's fluid from a non-isothermal wedge," *Ain Shams Engineering Journal*, vol. 8, no. 2, pp. 145–162, 2017.